Electronic Properties of Ultrathin InGaN/GaN Heterostructures under the Influences of Laser and Electric Fields

Investigation of the Harmonic and Inharmonic Potentials

En-nadir, Redouane; El Ghazi, Haddou; Basyooni, Mohamed A.; Tihtih, Mohammed; Belaid, Walid; Abboudi, Hassan; Maouhoubi, Ibrahim; Rabah, Mohamed; Zorkani, Izeddine

DOI
10.1016/j.physe.2024.115933

Publication date
2024

Document Version
Final published version

Published in
Physica E: Low-Dimensional Systems and Nanostructures

Physica E 160 (2024) 115933

Contents lists available at ScienceDirect

Physica E: Low-dimensional Systems and Nanostructures

journal homepage: www.elsevier.com/locate/physe

Electronic Properties of Ultrathin InGaN/GaN Heterostructures under the Influences of Laser and Electric Fields: Investigation of the Harmonic and Inharmonic Potentials

Redouane En-nadir [a,*], Haddou El Ghazi [a,b], Mohamed A. Basyooni-M. Kabatas [d,e], Mohammed Tihtih [c], Walid Belaid [d], Hassan Abboudi [a], Ibrahim Maouhoubi [a], Mohamed Rabah [a,b], Izeddine Zorkani [a]

[a] University of Sidi Mohamed Ben Abdullah, Fez B.P. 2202, Morocco
[b] ENSAM, University Hassan-II University, Casablanca, 20670, Morocco
[c] Institute of Ceramic and Polymer Engineering, University of Miskolc, Miskolc, 3515, Hungary
[d] Department of Precision and Microsystems Engineering, Delft University of Technology, Mekelweg 2, 2628 CD, Delft, Netherlands
[e] Department of Nanotechnology and Advanced Materials, Graduate School of Applied and Natural Science, Selçuk University, Konya, 42030, Turkey

ARTICLE INFO

Handling editor: M.W. Wu

Keywords:
Nanostructures
Binding-energy
Diamagnetic-susceptibility
Harmonicity
Probability-distribution
Intense external fields

ABSTRACT

Defects and impurities within semiconductor materials pose significant challenges. This investigation scrutinizes the response of a single dopant donor impurity located in nanostructured semiconductors, specifically quantum wells subjected to both harmonic and inharmonic confinement potentials. The primary focus of this inquiry centers on the analysis of binding energy, electron probability distribution, and diamagnetic susceptibility in connection with both the ground (1s) and excited (2p) electron states. Utilizing advanced computational techniques, specifically the Finite Elements Method (FEM) implemented through Python code, this study unveils a marked alteration in the interaction between electrons and impurities when exposed to external fields. Significantly, the characteristics of the confinement potential exert a substantial influence on the explored physical parameters. This research significantly advances our understanding of the interaction between impurities and intense fields, offering valuable insights into solid-state phenomena within low-dimensional systems. Consequently, it contributes to the design and fabrication of next-generation applications in the field of quantum well systems, encompassing areas such as lighting, detection, information processing, sensing, and energy conversion.

1. Introduction

The exploration of binding energies, impurity states and the responsiveness of nanostructured semiconductors to excitations, particularly their susceptibility within quantum wells has proven to be a fascinating pursuit in the large field of quantum physics [1,2]. These extraordinary structures, which are made up of incredibly thin layers with specific electrical characteristics, have proven to be an ideal setting for studying how matter behaves at the nanoscale. In this paper, we investigate the substantial impacts of both harmonic and inharmonic potentials on the ground and the first excited-state binding energies of single dopant donor-impurities emerging in quantum wells. We also reveal the fascinating interaction between these impurities and the dynamic interferences of strong electric and laser fields, which boosts the system complexity and opens up possibilities for emergent phenomena. The unique characteristics of quantum wells, with their confined electronic states and discrete energy levels, allow for the meticulous study of impurity behavior u [3].

III-nitride semiconductors, such as InN, GaN, and InGaN, stand at the forefront when it comes to fully leveraging the potential of quantum wells, offering numerous advantages [4]. These exceptional materials exhibit wide band-gaps, exceptional crystalline quality, and significant electron and hole mobility. Electron mobilities can reach several thousand cm^2/Vs, while hole mobilities typically range from tens to hundreds of cm^2/Vs. GaN, with its wider bandgap of approximately 3.4 eV, facilitates efficient light emission across the ultraviolet and visible spectrum. In contrast, InN boasts a smaller bandgap of about 0.7–0.9 eV [5]. These enticing properties of III-nitride semiconductors make their

* Corresponding author.
E-mail address: redouane.en-nadir@usmba.ac.ma (R. En-nadir).

https://doi.org/10.1016/j.physe.2024.115933
Received 13 October 2023; Received in revised form 5 January 2024; Accepted 17 February 2024
Available online 19 February 2024

quantum wells an attractive platform for groundbreaking optoelectronic devices, high-power lasers, solid-state lighting applications, and the exploration of impurity behavior [6].

The ground and first excited-state binding energies of single doping donor-impurities play a pivotal role as crucial indicators of stability and provide invaluable insights into the fundamental mechanisms governing these systems [7,8]. In the intricate world of quantum wells (QWs) and quantum dots (QDs), unraveling the complex dynamics heavily relies on understanding the intricate interplay between impurities and the potential landscape they inhabit that affect their electronic and optical properties [9–21]. In a QW, the confinement of electrons gives rise to harmonic potentials (HP) which behave like a harmonic oscillator, resulting in altered electrical characteristics and the emergence of quantized energy levels.

The introduction of inharmonic potentials (IHP) disrupts this idealized scenario, leading to complex energy landscapes and opening the door to intriguing phenomena [22]. The interaction between harmonic and inharmonic potentials within quantum wells offers a rich avenue to explore new behaviors and phenomena in these systems. When studying impurity donors in low-dimensional systems, such as QWs and QDs, researchers have mainly directed their attention to the ground state properties of these nanostructures [11–14]. While the ground state offers fundamental insight into electronic stability and structure, less emphasis has been placed on studying excited states in these analyses. Excited states, characterized by the promotion of electrons to higher energy levels, possess the potential to significantly influence the optical and electrical characteristics of QWs and QDs [23].

To better understand the behavior and dynamics of impurity donors within these nanostructures, we have to explore the excited states as well. This exploration will provide essential information needed for the design and optimization of highly efficient optoelectronic devices in the future. Furthermore, when a nano-crystal is exposed to intense laser and electric fields, the attractive forces within the quantum wells are further amplified. Application of an intense laser field helps stimulate non-equilibrium dynamics in the quantum well, giving rise to a host of phenomena including excitations, tunneling and even electron transfer between impurity states. Simultaneously, the presence of an electric field exerts a control on the binding energies and leads to changes in the behavior of the impurities in new ways [16–22,24]. Furthermore, extensive investigations have been conducted on the diamagnetic susceptibility of multiple nanostructured III-V (III–N)-based semiconductors with different geometries and potential shapes, including quantum wells, quantum dots, and quantum disks, under various influences and effects [23,25–29].

By combining the effects of these powerful external fields, we unlock the potential to explore a rich landscape of quantum phenomena and manipulate the behavior of impurities within the quantum well system. This paper delves into the examination of binding energies in quantum wells, specifically focusing on the ground and excited-state binding energies of single dopant donor-impurity. Through meticulous analysis and theoretical investigations, our aim is to shed light on the impact of both harmonic and inharmonic potentials on these binding energies. Additionally, we explore the responsiveness of InGaN based nanostructured semiconductors to excitations, particularly their susceptibility. Furthermore, we uncover the intricate interplay between these impurities and the captivating effects induced by intense laser and electric fields, which create an intriguing environment ripe for new discoveries. The numerical results presented in this paper have been obtained using the finite elements method, which is considered a powerful method compared to conventional frequently used methods such as vibrational and disruptive methods. The findings are analyzed and visualized utilizing Python libraries such as SciPy, NumPy, and Matplotlib.

2. Theory

In this study, we considered a single dopant donor impurity located at the center of a $GaN/In_{0.1}Ga_{0.9}N/GaN$ nanostructure, quantum well (QW), which is defined as $Z_0 = L + l/2$ with L represents the barrier's width while l denotes the well thickness, as shown in Fig. 1. The QW is made out of two different materials with distinct band gaps to confine the particles (electrons, holes). GaN was used as the material for the barriers, while InGaN served as the material for the well region. Within the framework of the effective mass theory, the Hamiltonian for an electron confined in a quantum well (QW) considering electron-impurity Colombian interaction and the electric field influence in one-dimensional can be expressed as follows:

$$H = -\frac{\hbar^2}{2}\vec{\nabla}\left(\frac{1}{m_e^*}\right)\vec{\nabla} + V_c(z) - \frac{e^2}{\varepsilon^*\left|\vec{r} - \vec{r}_0\right|} + e\xi(Z - Z_0) \tag{1}$$

$\hbar$, m_e^* and ε^* represent the Planck constant, electron effective mass, and the relative dielectric constant-related to the employed semiconductors, respectively. The electron-impurity distance is given as $\left|\vec{r} - \vec{r}_0\right| = \sqrt{(Z - Z_0)^2 + Y^2 + X^2}$, to simplify our calculations, we utilized a 1D-QW system; therefore, $Y = X = 1$. ξ denotes the applied electric field. The electron is confined in only one dimension, which is along the growth direction, Z-axis. V_c illustrates the confinement potential energy. In our calculations, we have taken some simplification on the electron wave functions by assuming X = 1 and Y = 1, effectively reducing the 3D problem to 1D, we wish to emphasize the physical rationale behind this choice. In many semiconductor nanostructures, such as quantum wells, the electron wavefunctions are strongly confined in one dimension due to quantum confinement effects. This confinement can significantly reduce the spread of the wavefunctions in the lateral (X and Y) directions, making the assumption of X = 1 and Y = 1 reasonable under certain conditions. Furthermore, this simplification aligns with the physical concept of quasi-1D systems, where the electron motion is predominantly along one direction (Z-direction) while being restricted in the other dimensions (X and Y).

The harmonic and Inharmonic potentials can be obtained from the following expression by adjusting its parameters, $\beta_1, \beta_2, \beta_3,$ and k [30–35].

$$V_c(z) = V_0\left[\beta_1\left(\frac{z}{k}\right)^2 + \beta_2\left(\frac{z}{k}\right)^4 + \beta_3\left(\frac{z}{k}\right)^6\right] \tag{2}$$

The initial depth of the QW is given by V_0, the well width is related to the parameters, $\beta_1, \beta_2, \beta_3,$ and k. The Harmonic potential (HP) can be obtained for $\beta_1 = 0.4, \beta_2 = \beta_3 = 0.1$ and $k = 1$ while the Inharmonic potential (IHP) is obtained with $\beta_1 = -1, \beta_2 = 1, \beta_3 = 0.1$ and $k = 1$. Furthermore, as β_1 increases, the well becomes narrower. The confinement potential can tuned to a single or double IHP depending on the values of the parameters β_2 and β_3.

The presence of impurities renders the Schrödinger equation unsolvable through analytical methods. As a solution, the Finite Elements Method (FEM) is employed, utilizing a one-dimensional mesh (calculation grid) consisting of $3N + 1$ points, with N set to 50. This approach provides accurate results for the ground state and low-lying excited states of simple quantum systems, such as the harmonic oscillator or the particle in a box. However, for more complex systems or higher excited states, the precision of the FEM solution may decrease due to the requirement of a finer mesh and higher-order basis functions. The accuracy of this method depends on the complexity of the problem, the selection of numerical parameters, and the availability of computational resources. Importantly, to obtain the energy levels and their corresponding wave functions, the one-dimensional Schrödinger equation along the z-axis is numerically solved, taking into account the following boundary conditions [36–38]:

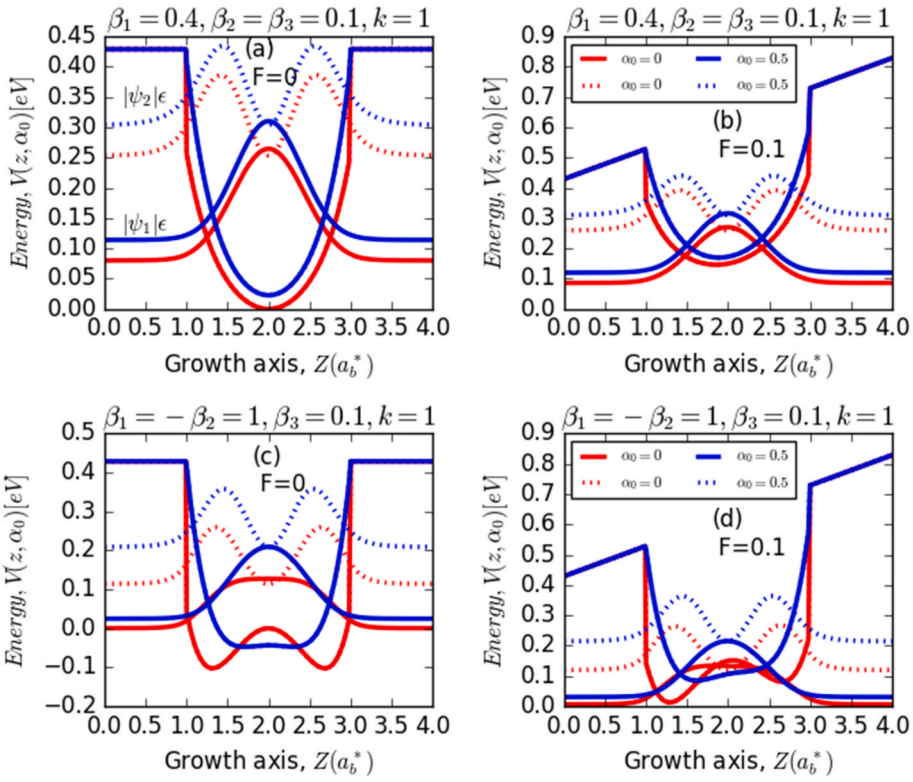

Fig. 1. Representation of the variation of electron probability densities for the 1s and 2p states of a GaN/InGaN quantum well (QW) with harmonic and inharmonic potentials, highlighting the impact of intense laser and electric fields. The potential profiles and corresponding ground-state wave functions are depicted by the red solid line ($\alpha_0 = 0$) for a harmonic potential and the blue solid line ($\alpha_0 = 0.5$) for an inharmonic potential. The second excited-state wave functions are represented by the dotted red line ($\alpha_0 = 0$) under a harmonic potential and the dotted blue line ($\alpha_0 = 0.5$) under an inharmonic potential.

$$\left[\underset{n}{\rightarrow}.\underset{\nabla}{\rightarrow}\left(\frac{\psi}{m^*_{e,b}}\right)\right]_b = \left[\underset{n}{\rightarrow}.\underset{\nabla}{\rightarrow}\left(\frac{\psi}{m^*_{e,w}}\right)\right]_w \tag{3}$$

The system under study utilizes a mesh grid composed of 3 N + 1 points. Each layer within the system is discretized with different step sizes. For the barriers, the step size is denoted as $h_b = \frac{L}{N}$, while for the regions within the well, it is represented as $h_w = \frac{l}{N}$. Consequently, for values of k ranging from 0 to N, the corresponding mesh nodes for a single quantum well can be determined as follows: the left barrier is located at $z_j = k * h_b$, the well region is situated at $z_j = L + k * h_w$, and the right barrier is positioned at $z_j = L + l + k * h_b$. By employing the FEM, the first and second derivative wave functions are calculated [39]:

$$\left.\frac{\partial^2\psi(z)}{\partial z^2}\right)_{z_k} = \frac{\psi_{k+1} - 2\psi_k + \psi_{k-1}}{(z_{k+1} - z_k)^2} \tag{4}$$

$$\left.\frac{\partial\psi(z)}{\partial z}\right)_{z_k} = \frac{\psi_{k+1} - \psi_k}{z_{k+1} - z_k} \tag{5}$$

Suppose that $h_b = z_{k+1} - z_k$, the equation (4) becomes as follows:

$$\left(\frac{-\hbar^2}{2\,m^*_{e,b}}\right)\left[\frac{\psi_{k-1} - 2\psi_k + \psi_{k+1}}{(h_b)^2}\right] + \left[V_c - \frac{e^2}{\varepsilon^*\left|\vec{r} - \vec{r}_0\right|} + e\xi(Z - Z_0)\right]\psi_k = E\,\psi_k \tag{6}$$

Assuming that $\Omega = \frac{-\hbar^2}{2\,m^* h_b^2}$ and $\delta = -\frac{e^2}{\varepsilon^*\left|\vec{r} - \vec{r}_0\right|} + e\xi(Z - Z_0)$, the same equation above becomes as follows:

$$\Omega\left[\psi_{k-1} + \psi_{k+1} + \left(\frac{V_c + \delta}{\Omega} - 2\right)\psi_k\right] = E\,\psi_k \tag{7}$$

in the barriers region, the matrix that provides the energy levels and corresponding wave functions in this particular region (barrier region) can then be written as follows:

$$\mathrm{M}^{\mathrm{Left,right}}_{\mathrm{Barrier}} = \begin{pmatrix} 0 & 0 & 0 & 0 & 0 & 0 \\ \Omega & (V_c + \delta - 2\Omega) & \Omega & 0 & 0 & 0 \\ 0 & \Omega & (V_c + \delta - 2\Omega) & \Omega & 0 & 0 \\ 0 & 0 & 0 & 0 & \ddots & \vdots \\ 0 & 0 & 0 & 0 & 0 & \cdots \\ 0 & 0 & 0 & 0 & 0 & 0 \end{pmatrix} \tag{8}$$

In the well region, the potential is zero ($V_0 = 0$). Thus, the matrix can be written as follows:

$$\mathrm{M}^{\mathrm{Middle}}_{\mathrm{well}} = \begin{pmatrix} 0 & 0 & 0 & 0 & 0 & 0 \\ \Omega & (\delta - 2\Omega) & \Omega & 0 & 0 & 0 \\ 0 & \Omega & (\delta - 2\Omega) & \Omega & 0 & 0 \\ 0 & 0 & 0 & 0 & \ddots & \vdots \\ 0 & 0 & 0 & 0 & 0 & \cdots \\ 0 & 0 & 0 & 0 & 0 & 0 \end{pmatrix} \tag{9}$$

The system's matrix is obtained by the sum of the matrix of different regions.

$$\mathrm{M}^{System}_{Nanostructure} = \mathrm{M}^{\mathrm{Left,right}}_{\mathrm{Barrier}} + \mathrm{M}^{Middle}_{well} \tag{10}$$

2.1. Intense laser field effect (ILF)

The effect of intense laser field (ILF) on the investigated system can be examined through the potential energy. According to the approach suggested by Lima et al. [28], a laser beam of single-color light, which

does not induce resonance, is directed parallel to the z-axis, the growth direction. This laser beam has a frequency of ω. Through the process described in Refs. [29,40,41], the intense terahertz (THz) laser alters the potential term, leading to the formation of a "dressed-laser" potential. The modified potential is derived by integrating Equation (6) over a single period of the laser field. The new form of potential is expressed as follows:

$$\langle V(z,\alpha_0)\rangle = \frac{\delta}{2\pi}\int_0^{\frac{2\pi}{\delta}} V(z+\alpha_0\sin(\delta t))dt, \tag{11}$$

Further details regarding the equations pertaining to dressed potentials and the non-perturbative approach utilizing the Kramers-Henneberger translation transformation to describe atomic behavior in the presence of intense high-frequency ILFs can be found in the Refs. [42]. The laser-dressing intensity parameter, denoted as α_0, is defined as $\frac{eF_0}{m^*\delta}$, where F_0 represents the magnitude of the laser field and e denotes the charge of an electron.

2.2. Electron probability density (PED)

The probability of locating the particle, specifically an electron, within the well region, can be determined by calculating the ratio of the probability of finding it within the well to the probability of finding it in the entire system. The analytical expression is provided as follows [43,44]:

$$P = 100\times\frac{\int_{\cdot}^{QW}|\Psi|^2dz}{\int_{\cdot}^{System}|\Psi|^2dz} \tag{12}$$

$$P = 100\times\frac{|<\psi_n^{Qw}|\psi_n^{Qw}>|^2}{|<\psi_n^{system}|\psi_n^{system}>|^2} \tag{13}$$

Where ψ_n^{QW} and ψ_n^{system} are respectively the wave functions corresponding to the electron within well region and the whole system, consequently. n is an integer ($n = 1,2,3,\ldots$) that indicates the energy level (i.e., electron state). Nevertheless, in this study, we are gripped only to the ground ($n = 1$) and first-excited ($n = 2$) electronic states.

2.3. 1s, 2p-states-related binding energy (BE)

The binding energy of the lowest (first-excited) states can be determined by taking into account the correlation between electrons and impurities in the system. It is calculated by subtracting the electron energy of the 1s and 2p states in the absence of the impurity (without impurity) from the corresponding energies in the presence of the impurity. This relationship can be expressed analytically as follows [24]:

$$E_{BE}^n = E_0^n - E_0^{n,Imp} \tag{14}$$

$$E_{BE}^n = \frac{<\psi_n|H_0|\psi_n>}{<\psi_n|\psi_n>} - \frac{<\psi_n|H_I|\psi_n>}{<\psi_n|\psi_n>} \tag{15}$$

where H_0 and H_I represent the electron Hamiltonians without and with the impurity, respectively. Whereas, ψ_n designates the 1s and 2p electron wave functions corresponding to $n = 1$ and $n = 2$ of the entire system.

2.4. Diamagnetic susceptibility

In the field of electromagnetism, the diamagnetic response quantifies the degree to which a semiconductor material becomes polarized or magnetized when subjected to an external electric, magnetic or laser field. Specifically, for a hydrogenic donor-impurity confined in a GaN/InGaN/GaN QW, the diamagnetic susceptibility (χ_{dia}) is analytically expressed in atomic units as follows [45–47]:

$$\chi_{dia} = -\frac{e^2}{6m_w^*(x)\varepsilon_w^{*2}(x)c^2}<Z^2> \tag{16}$$

where $<Z^2> = \frac{<\psi_n|Z^2|\psi_n>}{<\psi_n|\psi_n>}$ while m_w^* and ε_w^* are the electron effective mass and relative dielectric constant in the materials that forms the well region, subsequently.

3. Results and discussion

Throughout the study, we maintained a constant value of indium composition ($x = 0.1$), which represents 10% of the total fraction in the ternary alloy ($In_xGa_{1-x}N$). We selected this value because fabricating high-quality thin films (heterostructures) based on InGaN/GaN with higher indium (In) composition ($x > 0.2$) becomes challenging due to the localization issues that arise at the interfaces between the well and barrier semiconductor materials. For a fixed indium composition value of $x = 0.1$, a bowing parameter, $b = 3.8$, and an offset parameter, $Q = 0.7$, the physical ingredients that are used to compute numerically the investigated electronic properties are given as follows: The highest of the potential barrier is $V_0 = 429.1\ meV$, the difference of energy between the barrier and the well materials is given by $\Delta E_g = 613\ meV$ with $\Delta E_g = E_g^{GaN} - E_g^{InGaN}$. The calculations are scaled using effective units: the effective Bohr radius, $a_{GaN}^*(a_b^*) = 2.55\ nm$, is used as the length unit, and the effective Rydberg, $R_{GaN}^*(R_b^*) = 29\ meV$, is used as the energy unit. The rest of physical parameters of the materials used in this study are listed within the Table 1. These ingredients are the same as those utilized in our previous researches [48–50]. In this study, F indicates the effective applied electric field strength and it is given by $F = \frac{e\xi a_{GaN}^*}{R_{GaN}^*}$..

Fig. 1 illustrates the variation of the electronic probability densities (EPDs) for the 1s and 2p states along the growth direction of a GaN/InGaN/GaN QW. The QW is subject to harmonic and inharmonic potentials. The figure examines the effects of intense laser field (ILF) and electric field (F) on EPDs inside the investigated system. It is evident that both the ILF and electric field have a significant impact on the EPDs of the system. Regardless of the applied electric field, increasing the ILF, $\alpha_0 : 0\rightarrow 0.5$, tunes the harmonic potentials, leading to a reduction in the confining region of the quantum well (panels (a, b)). As a result, the EPDs related to the 1s and 2p states become more localized inside the well region, and their energy levels show a significant improvement.

Additionally, panels (c, d) demonstrate that in the presence of an ILF of the same intensity, the laser has caused deformation of the initial harmonic potential (IHP), transforming it into a quasi-harmonic potential. It is evident that when the ILF intensity is non-zero, the EPDs associated with the 1s and 2p states become more localized towards the center within the well region, and their energy levels exhibit a significantly enhanced behavior. This is due to the improvement in the quantum confinenmt under the influence of the ILF. However, it is observed that the introduction of an applied electric field has a significant impact on both the HP and the IHP, consequently affecting the EPDs. It is demonstrated that as the electric field intensity (F) increases from 0 to 0.1, both the HP and IHP undergo deformation. As a result, the EPDs become silighly localized within the left-side region of the well compared to the righ-side of the well. This phenomenon can be explained by the fact that the electric field compels the charges to move in the opposite direction of the applied electric field, which is applied

Table 1
Distinctive features of InN, GaN, and their ternary alloy InGaN semiconductor materials [51].

Parameters	GaN	InN	InGaN
Band gap at T = 300K, E_g(eV)	3.41	0.7	2.797
Electron effective mass (m_0)	0.20	0.11	0.17
Dielectric constant (ε_0)	9.6	10.5	10.24

from the structure's origin (Z = 0). These results are essential for interpreting the binding energy and diamagnetic susceptibility of a mobile donor impurity initially located at the center of the studied system, quantum well (QW).

Fig. 2 illustrates the changes in electron presence probabilities (EPPs) corresponding to the 1s and 2p states within the QW as a function of the intense laser field. The QW is modeled using both harmonic and inharmonic potentials, including the impact of an applied electric field on these EPPs. Panel (a) show the influence of eletric field on the ground state-related PEPD in the HP. It reveals that the presence electron probability density (PEPD) associated with the 1s state in a harmonic potential (HP) increases proportionally with the strength of the intense laser field (ILF). As the ILF strength increases, the PEPD becomes more pronounced. Additionally, it is observed that increasing the applied electric field also enhances the PEPD. This can be attributed to the fact that with increasing ILF intensity, the electron wave function becomes more localized within the well region, leading to a notable increase in its PEPD. Similarly, under an intense electric field, the PEPD is further improved because a stronger electric field results in even greater localization of the electron wave function within the well region. Therefore, the PEPD can only increase in this case.

Similarly, in panel (b), plots the influence of eletric field on the ground state-related PEPD in the IHP. It demonstartes that the PEPD increases accordingly with the ILF intensity and reaches a saturation regime for higher ILF values (ILF >0.8). This can be attributed to the reduction in the IHP harmonicity and the reduction in spatial confinement, which provide a higher probability for an electron to be localized inside the well region compared to the barrier regions. Moreover, it is observed that the PEPD is improved as the intensity of the applied electric field increases, especially in the range of the lower values of the ILF intensities (ILF <0.5). This behavior is related to the fact that the electron ground state related-PEPD becomes less sensitive to an applied external electric field in the case of higher ILF intensities.

A similar behavior is observed in panel (b), except that in this panel, the influence of the applied electric field is more pronounced in the higher range of ILF. This can be explained by the fact that in this range of ILF, the PEPD associated with the first-excited state of the electron becomes more sensitive to an applied electric field compared to lower ILF intensities. Moreover, panel (c) illustrates the effect of appllied eletric field on the first-excited state-related PEPD in the HP. It reveals that the PEPD-related 2p-state in HP remains constant for all values of ILF below approximately 0.5, and then drops dramatically. This behavior is associated to the insensitivity of the PEPD-related 2p-state in HP to the induced ILF intensity in this range. Additionally, regardless of the ILF intensity, the PEPD-related 2p-state in HP improves under an applied electric field. This improvement can be explained by the fact that the applied electric field dominates and affects the PEPD-related 2p-state, enhancing it in the case of HP. Furthermore, panel (d) depicts the impact of appllied eletric field on the first-excited state-related PEPD in the IHP. It is clear that the PEPD-related 2p-state improves with an increase in the applied ILF until it reachs a stable regime. Furthermore, its enhancement is more pronounced with higher intensities of the applied electric field. This effect becomes particularly prominent with higher ILF values in comparison to lower ones. This can be attributed to the fact that an increase in the applied electric field enhances the charge distribution within the well, subsequently leading to an improvement in the PEPD-related 2p-state.

Fig. 3 shows the variation in the binding energy (BE) of the donor impurity related to 1s and 2p electronic states in response to simultaneous variations of the electric and laser fields. The 3D plot (panesl: a,b, c,d) highlights the differences between the Harmonic and Inharmonic potential scenarios.

Panel (a) illustrates the variation in the 1s-related BE within HP versus to electric field (x-axis) and ILF (y-axis). It is shown that both fields have a significant impact on the BE. The BE of this latest system increases smoothly with the applied electric field due to the reduction in the electron-impurity distance, leading to an improvement in the Coulomb interaction. As a result, the binding energy can only increase.

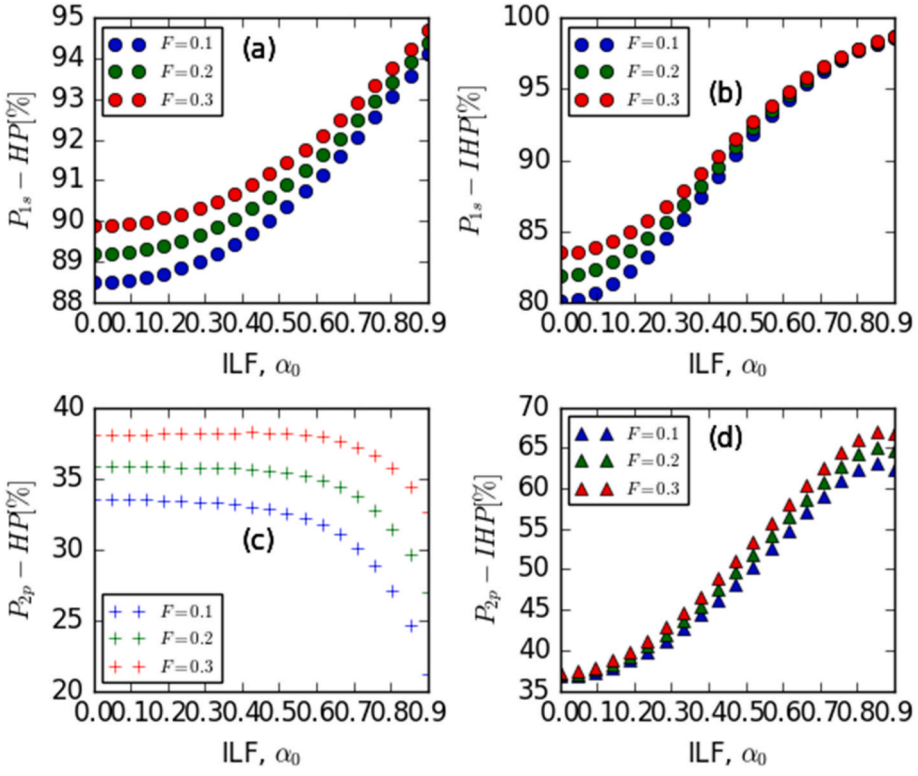

Fig. 2. Variation of the electron probability-related 1*s* and 2*p* states inside the QW versus the intense laser field with Harmonic and Inharmonic potentials: Effect of the applied electric field.

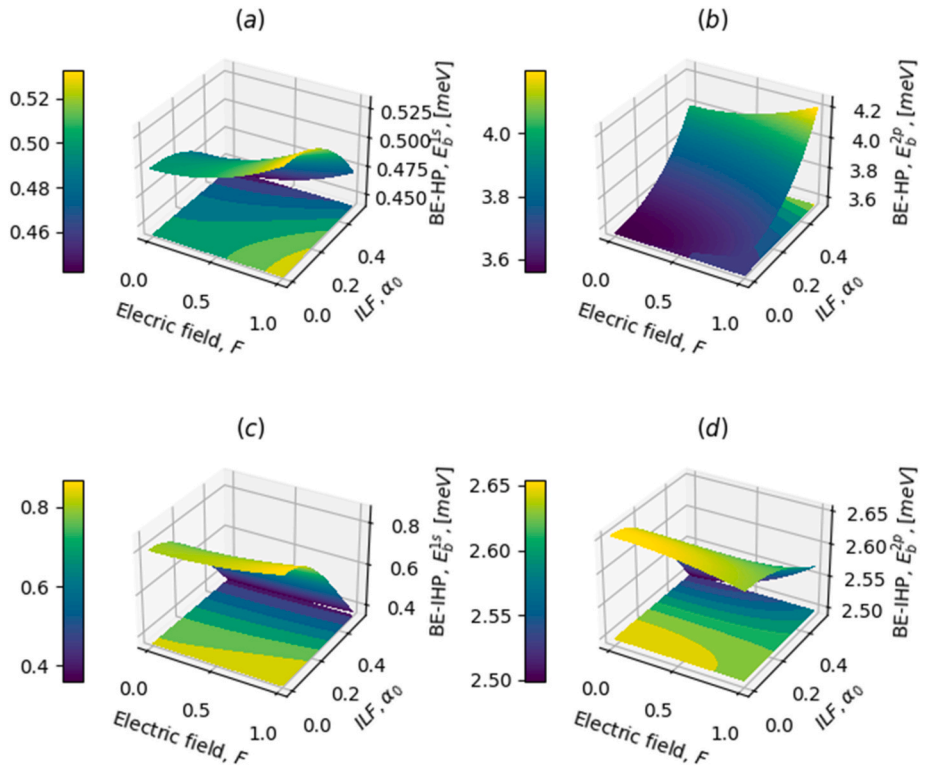

Fig. 3. The variation of 1*s* and 2*p*-states-related donor-impurity binding energy versus applied electric field (x-axis) and intense laser field (y-axis) considering Harmonic and Inharmonic potentials.

In contrast, the same panel shows that the BE decreases with increasing ILF intensity. This can be explained by the fact that as the ILF intensity increases, the electron-impurity separation also increases, leading to a decrease in the electron's BE in this situation. In this case, the estimated highest value of the electron BE is approximately 0.52 *meV*, while the lowest value is around 0.46 *meV*, resulting in a shift of approximately 0.06 *meV*.

Panel (b) plots the variation in the BE of the electron related to the 2p state within the harmonic potential (HP) as a function of the applied electric field strength (x-axis) and ILF intensity (y-axis). It is evident from this panel that both fields have a remarkable effect on the BE of the electron. The impact of the ILF intensity is more pronounced compared to that induced by an externally applied electric field. The BE shows a slight increase under the applied electric field, while a rapid improvement is observed with increasing ILF intensity. The physical reason behind this behavior is that within the HP, the intensity of the ILF dominates over the applied electric field strength. As a result, the BE related to the 2p-state is more affected by the applied electric field compared to the ILF. In this scenario, the BE has reached a maximum value estimated at 4.2 *meV* and a minimum value of around 3.6 *meV*, resulting in a significant shift of approximately 0.6 meV. Now, let's examine the behavior of the electron's binding energy (BE) considering an inharmonic potential (IHP).

Panel (c) illustrates the variation in the BE related to the 1s-state within the IHP with respect to an applied electric field (x-axis) and ILF (y-axis). It is evident that both fields have a significant impact on the binding energy (BE), with the ILF exerting a particularly noticeable effect. It can be observed from this panel that the BE increases slightly with the applied electric field, while it undergoes a drastic decrease with increasing ILF intensity. In this potential, the increase in the ILF restricts the electron within the potential, making it less sensitive to an applied electric field. However, the increase in ILF intensity reduces the width of the potential, leading to enhanced spatial confinement. This confinement forces the electron to spread towards the barriers material, thereby reducing the electron-impurity distance. Consequently, the reduction in the electron-impurity distance results in a decrease in its BE. In this scenario, the electron's BE reached a maximum value of approximately 0.8 *meV* and a minimum value of around 0.4 *meV*, resulting in a shift estimated to be approximately 0.4 *meV*.

Considering the same inharmonic potential (IHP), panel (d) displays the variation in the binding energy (BE) of the electron related to the 2p-state as a function of the applied electric field strength (x-axis) and ILF intensity (y-axis). It is evident from this panel that the BE of the electron related to the 2p state is significantly affected by both the applied electric field and ILF. The BE is reduced under both fields, but the decrease is more pronounced under the ILF compared to the impact of the applied electric field. This decrease in the BE is attributed to the improvement in the electron-impurity distance under both fields, leading to a reduction in the Coulomb interaction between the electron and the impurity. In this type of potential, the applied electric field attracts the electron away from the impurity, increasing their separation distance. Additionally, the ILF forces the electron to move towards the edges of the system, further enhancing the distance between the electron and the impurity. As a result, the binding energy can only diminish. In this case, the electron's BE reached a maximum value of approximately 2.65 *meV* and a minimum value of around 2.50 *meV*, resulting in a shift estimated to be approximately 0.15 *meV*. The positioning of impurities within the system plays a critical role in determining the electron binding energy (BE) of the studied system. To explore this influence, we examine the variation of binding energy related to 1s and 2p states-associated donor impurity as a function of impurity location within the system.

Fig. 4 showcases this variation, considering both the Harmonic (HP) and Inharmonic (IHP) potentials. It is well noticed from panel (a,b) that the impurity position within the system has a remarkable impact on the electron's BE related to both 1s and 2p states with the two investigated potentials. Regardless the potentials and without the applied electric field and ILF intensity, the BE related to the 1s and 2p states is lowest

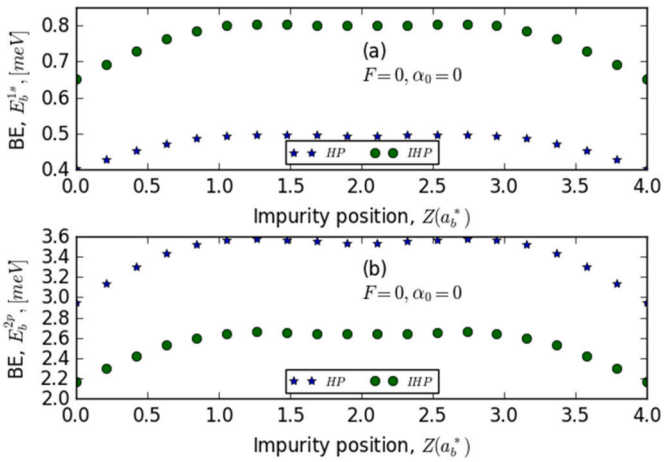

Fig. 4. The variation of 1*s* and 2*p*-states-related donor-impurity binding energy versus the impurity-location within the system: Effects of the Harmonic and Inharmonic potentials are considered.

around the center of the structure, while it is highest near the edges of the system. This phenomenon can be explained by the fact that as the electron approaches the center of the system, the Coulomb interaction becomes more significant due to the reduced electron-impurity distance. Consequently, the BE becomes more pronounced in these areas of space. However, the slight decrease in the BE observed at the center of the nanostructure. This can be attributed to the fact that as the electron occupies the central region of the system, its energy increases. Consequently, the electron has a tendency to escape from the well region and move towards the barrier materials. As a result, the Coulomb interaction between the electron and the impurity diminishes due to the improved separation of their distance. This leads to a slight reduction in the BE. Furthermore, it is crucial to note that for all impurity positions, the BE associated with both 1s and 2p states is higher in the case of an IHP compared to the HP. This observation suggests that the probability of removing the electron from the impurity is reduced with an IHP in contrast to an HP. In the absence of any excitation, the electron is compelled to stay near the impurity, leading to an elevation in its BE. After having thoroughly discussed the binding energy (BE) associated with a single donor impurity in GaN/InGaN nanostructures, we will now explore the diamagnetic susceptibility (DS) pertaining to this donor impurity within the same investigated system. This physical parameter quantifies the capacity of the donor impurity to generate a response when subjected to external excitations, such as electric or intense laser fields. It provides insight into the degree to which the donor impurity either resists or reacts to these excitations.

Fig. 5 illustrates the impact of electric and intense laser fields on the changes in DS associated with the 1s and 2p orbitals of donor impurity emerged at the center of the system. The panels (a, b, c, d) represent this variation for two distinct potential profiles, namely IHP and HP.

Panel (a) reveals a gradual rise in the DS related to 1s-orbital with a HP as the intense laser field (ILF) increases, whereas a notable surge occurs with an elevation in the applied electric field. This behavior can be associated to the growing influence of the system's response to external excitation as the ILF intensity strengthens. Furthermore, the enhancement in electric field strength amplifies this responsiveness even further. For high ILF intensities (ILF > 0.5), the observed amplification was diminished.

Panel (b) displays the change in DS associated with the 1s-orbital, taking into account an IHP versus the ILF for three distinct values of the applied electric field. It is evident that the DS exhibits a similar pattern of increase with increasing ILF intensities, as observed in the HP. In addition, the DS experiences a jump to higher values with the improvement of electric field strength. Although, this enhancement is less prominent for higher ILF intensities. This is due to the fact that as the ILF intensity increases, the system's response becomes less sensitive to an external electric field, thereby reducing its impact.

Panel (c) showcases the variation of the DS associated with the 2s-orbital in the presence of an HP, considering different intensities of the applied electric field. The DS exhibits changes as a function of the ILF for each applied electric field intensity. The observed behavior in panel

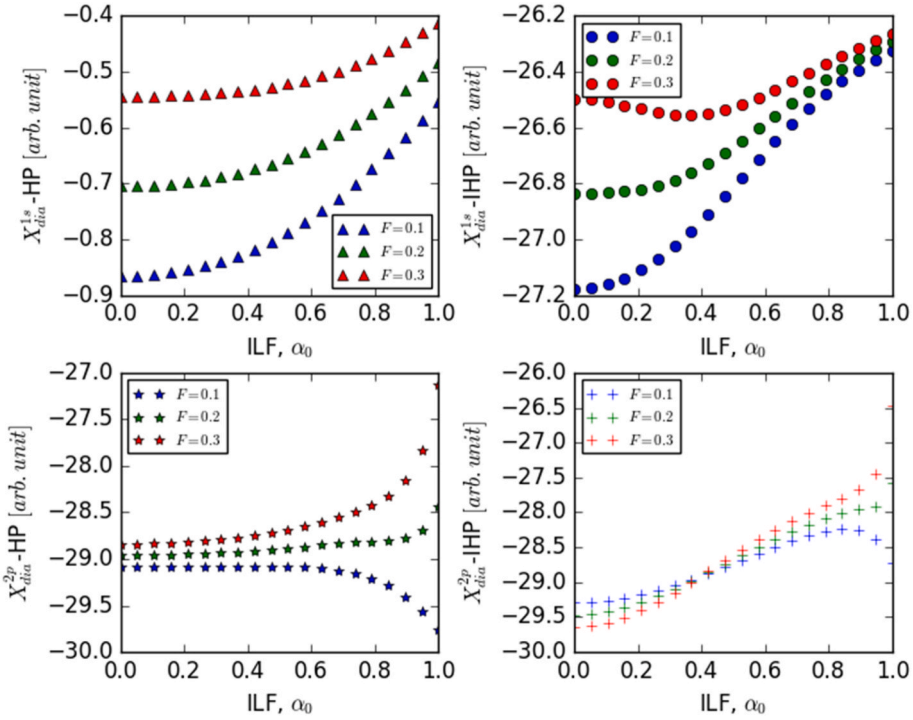

Fig. 5. The variation of 1*s* and 2*p*-states-related donor-impurity diamagnetic susceptibility versus applied intense laser field considering Harmonic and Inharmonic potentials: Effects of applied electric field.

(c) reveals that the DS remains relatively constant for weaker ILF intensities. However, for higher ILF intensities (ILF $>$ 0.6), the DS experiences a significant increase/decrease, depending on the strength of the applied electric field. The panel indicates that for electric field intensities below 0.2 (F $<$ 0.2), there is a rapid decrease in the DS. This suggests that the system's responsiveness to an excitation weakens at lower electric field intensities. However, for intensities higher than 0.2 (F $>$ 0.2), the DS is enhanced, indicating an increased system responsiveness to the applied electric field. In panel (d), the evolution of the DS linked with the 2s-orbital is depicted within an IHP. The DS is examined for various intensities of the applied electric field, providing insight into the impact of the electric field on the system's DS response. The panel demonstrates that the DS presents two distinct behaviors. For lower ILF intensities, the system's DS remains relatively constant in panel (d). However, as the ILF intensity increases and reaches a critical value, the DS starts to decrease. This drop is particularly notable for lower values of the applied electric field (F $<$ 0.1). Moreover, it is important to notice that the DS is not affected by the applied electric field for a critical values of the ILF around 0.45 (ILF $\approx$ 0.45). At this critical point, the system becomes less sensitive to the applied electric field, resulting in a reversal of the behavior of the DS. Interestingly, the DS exhibits higher values for lower electric field intensities, but as the ILF intensity increases, it becomes lower for weaker values of the applied electric field.

Comparing our findings, particularly the donor-impurity binding energy (BE) and its related diamagnetic susceptibility (DS) associated with the ground and first excited states (1s and 2p hybridization), with experimental and theoretical results, proved challenging due to the specific choice of the investigated system and its unique geometrical and physical properties. Furthermore, the influence of the electric field and intense laser field (ILF), which are rarely considered in similar studies, further complicated the comparison. The distinct characteristics of the system and the incorporation of these fields presented limitations in directly aligning our findings with existing research. Nonetheless, this study provides valuable insights that contribute to improving our understanding of these parameters, thereby advancing both theoretical and experimental aspects of the field.

4. Conclusions

This research delves into the challenges presented by impurities in semiconductors and explores the profound impact of intense laser and electric fields on the binding energy (BE) and diamagnetic susceptibility (DS) of single dopant donor impurities within quantum wells (QWs), considering both harmonic potential (HP) and inharmonic potential (IHP). With a specific focus on the 1s and 2p electron states, the study elucidates the influence of external intense fields on both BE and DS, revealing remarkable shifts when transitioning from HP to IHP. Furthermore, it underscores the significant impact of external fields on electron-impurity correlations and the probability distributions within the quantum well (QW), offering comprehensive insights into the behavior of nanostructured semiconductors under high-intensity conditions. Consequently, it reveals the diverse potential applications of InGaN/GaN quantum well systems, spanning LEDs, laser diodes, solar cells, optical sensors, high-frequency electronics, UV photodetectors, biomedical imaging, greenhouse lighting, quantum cascade lasers, quantum computing, and solid-state lighting.

Institutional review board statement

Not applicable.

Informed consent statement

Not applicable.

Funding

Not applicable.

CRediT authorship contribution statement

Redouane En-nadir: Conceptualization, Formal analysis, Investigation, Methodology, Project administration, Resources, Software, Writing – original draft. **Haddou El Ghazi:** Conceptualization, Formal analysis, Supervision, Validation, Writing – review & editing. **Mohamed A. Basyooni-M. Kabatas:** Conceptualization, Formal analysis, Investigation, Methodology, Writing – review & editing. **Mohammed Tihtih:** Conceptualization, Data curation, Writing – review & editing. **Walid Belaid:** Conceptualization, Formal analysis, Software, Writing – original draft, Writing – review & editing. **Hassan Abboudi:** Conceptualization, Formal analysis, Writing – original draft. **Ibrahim Maouhoubi:** Methodology, Writing – original draft. **Mohamed Rabah:** Investigation, Methodology, Resources. **Izeddine Zorkani:** Supervision, Validation, Writing – review & editing.

Declaration of competing interest

The authors declare that they have no known competing financial interests or personal relationships that could have appeared to influence the work reported in this paper.

Data availability

No data was used for the research described in the article.

Acknowledgements

The authors would like to express their sincere gratitude to Professors Hamdi Şükür Kılıç from Selçuk University, Konya, Turkey, and Ramazan Yasin from Necmettin Erbakan University, Konya, Turkey, for their valuable contributions and insightful discussions throughout the project. Their availability and expertise greatly helped enhance the quality of the work. Additionally, we acknowledge the International Center for Theoretical Physics (ICTP) in Trieste, Italy, for their support and encouragement for researchers from developing countries such as Morocco.

References

[1] D.T. Thoai, R. Zimmermann, M. Grundmann, D. Bimberg, Image charges in semiconductor quantum wells: effect on exciton binding energy, Phys. Rev. B 42 (9) (1990) 5906.
[2] A. Lewicki, J. Spalek, A. Mycielski, Magnetic susceptibility and specific heat of the semi-magnetic semiconductors Cd1-xFexSe and Hg1-xFexSe and their mixtures, J. Phys. C Solid State Phys. 20 (13) (2005), 1987.
[3] E.E. Mendez, K. von Klitzing, Physics and Applications of Quantum Wells and Superlattices, vol. 170, Springer Science & Business Media, 2012.
[4] M. Beeler, E. Trichas, E. Monroy, III-nitride semiconductors for intersubband optoelectronics: a review, Semicond. Sci. Technol. 28 (7) (2013) 074022.
[5] S.N. Mohammad, H. Morkoç, Progress and prospects of group-III nitride semiconductors, Prog. Quant. Electron. 20 (5) (Jan. 1996) 361–525, https://doi.org/10.1016/S0079-6727(96)00002-X.
[6] M. Henini, M. Razeghi, Optoelectronic Devices: III Nitrides, Elsevier, 2004.
[7] A. Mauger, J.C. Bourgoin, Relationship between donor defects and band structure in III-V alloys, Phys. Rev. B 46 (19) (1992) 12278.
[8] K. Ploog, G.H. Döhler, Compositional and doping superlattices in III-V semiconductors, Adv. Phys. 32 (3) (1983) 285–359.
[9] A. Amthong, WKB approximation for abruptly varying potential wells, Eur. J. Phys. 35 (6) (2014) 065009.
[10] E. Kasapoglu, et al., Combined effects of intense laser field, electric and magnetic fields on the nonlinear optical properties of the step-like quantum well, Mater. Chem. Phys. 154 (2015) 170–175.
[11] F. Ungan, R.L. Restrepo, M.E. Mora-Ramos, A.L. Morales, C.A. Duque, Intersubband optical absorption coefficients and refractive index changes in a graded quantum well under intense laser field: effects of hydrostatic pressure, temperature and electric field, Phys. B Condens. Matter 434 (Feb. 2014) 26–31, https://doi.org/10.1016/j.physb.2013.10.053.

[12] C.A. Duque, N. Porras-Montenegro, Z. Barticevic, M. Pacheco, L.E. Oliveira, Electron-hole transitions in self-assembled InAs/GaAs quantum dots: effects of applied magnetic fields and hydrostatic pressure, Microelectron. J. 36 (3–6) (2005) 231–233.

[13] H. Odhiambo Oyoko, N. Porras-Montenegro, S.Y. López, C.A. Duque, Comparative study of the hydrostatic pressure and temperature effects on the impurity-related optical properties in single and double GaAs–Ga $_{1-}$ x Al x as quantum wells, Phys. Status Solidi C 4 (2) (Feb. 2007) 298–300, https://doi.org/10.1002/pssc.200673259.

[14] C.M. Duque Jiménez, C.A. Duque Echeverri, M.G. Barseghyan, Donor Impurity in Vertically-Coupled Quantum-Dots under Hydrostatic Pressure and Applied Electric Field, 2010. Accessed: Jan. 05, 2024. [Online]. Available: https://bibliotecadigital.udea.edu.co/handle/10495/31003.

[15] C.A. Duque, E. Kasapoglu, S. Sakiroglu, H. Sari, I. Sökmen, Intense laser effects on donor impurity in a cylindrical single and vertically coupled quantum dots under combined effects of hydrostatic pressure and applied electric field, Appl. Surf. Sci. 256 (24) (Oct. 2010) 7406–7413, https://doi.org/10.1016/j.apsusc.2010.05.081.

[16] R. En-nadir, et al., Enhancing emission via Radiative lifetime manipulation in ultrathin inGaN/GaN quantum wells: the effects of simultaneous electric and magnetic fields, thickness, and impurity, Nanomaterials 13 (Jan. 2023) 21, https://doi.org/10.3390/nano13212817. Art. no. 21.

[17] R. En-nadir, H. El Ghazi, A. Jorio, I. Zorkani, Inter and intra band impurity-related absorption in (In, Ga) N/GaN QW under composition, size and impurity effects, in: MATEC Web of Conferences, EDP Sciences, 2020.

[18] R. En-nadir, H. El Ghazi, A. Jorio, I. Zorkani, H. Kiliç, Intersubband optical absorption in (In,Ga)N/GaN double quantum wells considering applied electric field effects, J. Comput. Electron. (Jan. 2022) 1–8, https://doi.org/10.1007/s10825-021-01830-4.

[19] R. En-nadir, M.A.B.-M. Kabatas, M. Tihtih, H.E. Ghazi, Linear and nonlinear optical absorption coefficients in InGaN/GaN quantum wells: interplay between intense laser field and higher-order anharmonic potentials, Heliyon 0 (0) (2023) e22867, https://doi.org/10.1016/j.heliyon.2023.e22867. Nov.

[20] W. Belaid, H. El Ghazi, R. En-Nadir, H.Ş. Kılıç, I. Zorkani, A. Jorio, Temperature-related electronic low-lying states in different shapes in. 1Ga. 9N/GaN double quantum wells under size effects, Trends Sci 19 (17) (2022), 5777–5777.

[21] W. Belaid, et al., A theoretical study of the effects of electric field, hydrostatic pressure, and temperature on photoionization cross-section of a donor impurity in (Al, Ga)N/AlN double triangular quantum wells, Phys. Scripta 98 (4) (Mar. 2023) 045913, https://doi.org/10.1088/1402-4896/acc5c0.

[22] C.W. Li, et al., Orbitally driven giant phonon anharmonicity in SnSe, Nat. Phys. 11 (12) (2015) 1063–1069.

[23] H. El Ghazi, A. Jorio, I. Zorkani, Impurity binding energy of lowest-excited state in (In, Ga) N–GaN spherical QD under electric field effect, Phys. B Condens. Matter 426 (2013) 155–157.

[24] R. En-Nadir, H. El Ghazi, A. Jorio, I. Zorkani, Ground-state shallow-donor binding energy in (in, Ga) N/GaN double QWs under temperature, size, and the impurity position effects, J. Model. Simul. Microsyst. 4 (1) (2021) 1–6.

[25] E.B. Al, E. Kasapoglu, S. Sakiroglu, C.A. Duque, I. Sökmen, Binding energy of donor impurity states and optical absorption in the Tietz-Hua quantum well under an applied electric field, J. Mol. Struct. 1157 (2018) 288–291.

[26] E.B. Al, E. Kasapoglu, S. Sakiroglu, H. Sari, I. Sökmen, Influence of position dependent effective mass on impurity binding energy and absorption in quantum wells with the Konwent potential, Mater. Sci. Semicond. Process. 135 (2021) 106076.

[27] A. Ed-Dahmouny, A. Sali, N. Es-Sbai, R. Arraoui, C.A. Duque, The impact of hydrostatic pressure and temperature on the binding energy, linear, third-order nonlinear, and total optical absorption coefficients and refractive index changes of a hydrogenic donor impurity confined in GaAs/Al x Ga1- x as double quantum dots, Eur. Phys. J. Plus 137 (7) (2022) 784.

[28] F.M.S. Lima, M.A. Amato, O.a.C. Nunes, A.L.A. Fonseca, B.G. Enders, E.F. da S. Jr, Unexpected transition from single to double quantum well potential induced by intense laser fields in a semiconductor quantum well, J. Appl. Phys. 105 (12) (Jun. 2009) 123111, https://doi.org/10.1063/1.3153963.

[29] E. Kasapoglu, H. Sari, I. Sökmen, J.A. Vinasco, D. Laroze, C.A. Duque, Effects of intense laser field and position dependent effective mass in Razavy quantum wells and quantum dots, Phys. E Low-Dimens. Syst. Nanostructures 126 (2021) 114461.

[30] A.-N. Aishah, H. Dakhlaoui, T. Ghrib, B.M. Wong, Effects of magnetic, electric, and intense laser fields on the optical properties of AlGaAs/GaAs quantum wells for terahertz photodetectors, Phys. B Condens. Matter 635 (2022) 413838.

[31] M. Bati, The effects of the intense laser field on the resonant tunneling properties of the symmetric triple inverse parabolic barrier double well structure, Phys. B Condens. Matter 594 (Oct. 2020) 412314, https://doi.org/10.1016/j.physb.2020.412314.

[32] M.J. Karimi, H. Vafaei, Intense laser field effects on the linear and nonlinear intersubband optical properties in a strained InGaN/GaN quantum well, Phys. B Condens. Matter 452 (2014) 131–135.

[33] M.E. Mora-Ramos, C.A. Duque, E. Kasapoglu, H. Sari, I. Sökmen, Linear and nonlinear optical properties in a semiconductor quantum well under intense laser radiation: effects of applied electromagnetic fields, J. Lumin. 132 (4) (Apr. 2012) 901–913, https://doi.org/10.1016/j.jlumin.2011.11.008.

[34] F. Ungan, U. Yesilgul, S. Şakiroğlu, E. Kasapoglu, H. Sari, I. Sökmen, Effects of an intense, high-frequency laser field on the intersubband transitions and impurity binding energy in semiconductor quantum wells, Phys. Lett. 374 (29) (2010) 2980–2984.

[35] A. Fakkahi, M. Kirak, A. Sali, Effect of impurity position and electric field on the optical absorption coefficients and oscillator strength in spherical multilayer quantum dot, Eur. Phys. J. Plus 137 (9) (2022) 1–19.

[36] I. Maouhoubi, R. En-nadir, I. Zorkani, A.O.T. Hassani, A. Jorio, The effects of the dielectric screening, temperature, magnetic field, and the structure dimension on the diamagnetic susceptibility and the binding energy of a donor-impurity in quantum disk, Phys. B Condens. Matter (2022) 414371.

[37] I. Maouhoubi, R. En-nadir, K. El Bekkari, I. Zorkani, A. Ouazzani Tayebi Hassani, A. Jorio, Effects of applied magnetic field and pressure on the diamagnetic susceptibility and binding energy of donor impurity in GaAs quantum dot considering the non-parabolicity model's influence, Philos. Mag. A 103 (3) (2023) 286–303.

[38] M. Solaimani, Binding energy and diamagnetic susceptibility of donor impurities in quantum dots with different geometries and potentials, Mater. Sci. Eng. B 262 (Dec. 2020) 114694, https://doi.org/10.1016/j.mseb.2020.114694.

[39] L.R. Ram-Mohan, S. Saigal, D. Dossa, J. Shertzer, The finite-element method for energy eigenvalues of quantum mechanical systems, Comput. Phys. 4 (1) (1990) 50–59.

[40] H. Dakhlaoui, J.A. Vinasco, C.A. Duque, External fields controlling the nonlinear optical properties of quantum cascade laser based on staircase-like quantum wells, Superlattice. Microst. 155 (Jul. 2021) 106885, https://doi.org/10.1016/j.spmi.2021.106885.

[41] M. Panda, T. Das, B.K. Panda, Nonlinear optical properties in the laser-dressed two-level AlxGa1−xN/GaN single quantum well, Int. J. Mod. Phys. B 32 (4) (Feb. 2018) 1850032, https://doi.org/10.1142/S0217979218500327.

[42] B. Pradhan, B.K. Panda, Effect of intense laser field in GaAs/Al x Ga1−x as quantum well, Adv. Sci. Lett. 20 (3–4) (Mar. 2014) 726–728, https://doi.org/10.1166/asl.2014.5365.

[43] R. En-nadir, et al., Exploring the electronic properties of shallow donor impurities in modified ∩-shaped potential: effects of applied electric field, parabolicity, compositions, and thickness, Eur. Phys. J. B 96 (Jun. 2023) 78, https://doi.org/10.1140/epjb/s10051-023-00539-6.

[44] H. El Ghazi, A. Jorio, I. Zorkani, E.M. Feddi, A. El Mouchtachi, Wetting layer effect on impurity-related electronic properties of different (In,Ga)N QD-shapes, Phys. B Condens. Matter 537 (May 2018) 207–211, https://doi.org/10.1016/j.physb.2018.02.028.

[45] R. En-nadir, et al., Tailoring optoelectronic properties of InGaN-based quantum wells through electric field, indium content, and confinement shape: a theoretical investigation, Phys. B Condens. Matter 663 (Aug. 2023) 414976, https://doi.org/10.1016/j.physb.2023.414976.

[46] R. En-nadir, et al., Analyzing the combined influences of external electric field, impurity-location, in-content, and QW's number on donor-impurity binding energy in multiple quantum wells with finite squared potential, Opt. Quant. Electron. 55 (7) (May 2023) 597, https://doi.org/10.1007/s11082-023-04893-8.

[47] H. El Ghazi, R. En-nadir, H. Abboudi, F. Jabouti, A. Jorio, I. Zorkani, Two-dimensional electron gas modeling in strained InN/GaN hetero-interface under pressure and impurity effects, Phys. B Condens. Matter 582 (Apr. 2020) 411951, https://doi.org/10.1016/j.physb.2019.411951.

[48] E. Iqraoun, A. Sali, K. El-Bakkari, M.E. Mora-Ramos, C.A. Duque, Binding energy, polarizability, and diamagnetic response of shallow donor impurity in zinc blende GaN quantum dots, Micro Nanostructures 163 (Mar. 2022) 107142, https://doi.org/10.1016/j.spmi.2021.107142.

[49] K. El-Bakkari, A. Sali, E. Iqraoun, A. Ezzarfi, Polaron and conduction band non-parabolicity effects on the binding energy, diamagnetic susceptibility and polarizability of an impurity in quantum rings, Superlattice. Microst. 148 (2020) 106729.

[50] R. En-nadir, Theoretical study of the non-parabolicity and size effects on the diamagnetic susceptibility of donor impurity in Si, HgS and GaAs cylindrical quantum dot and quantum disk: applied magnetic field influence is considered, Philos. Mag. A (Dec. 2022) 1, https://doi.org/10.1080/14786435.2022.2158384. –14.

[51] H. Abboudi, H. EL Ghazi, R. En-nadir, M.A. Basyooni-M. Kabatas, A. Jorio, I. Zorkani, Efficiency of InN/inGaN/GaN intermediate-band solar cell under the effects of hydrostatic pressure, Compositions, Built-in-Electric Field, Confinement, and Thickness', Nanomaterials 14 (1) (Jan. 2024), https://doi.org/10.3390/nano14010104. Art. no. 1.